JACS
JOURNAL OF THE AMERICAN CHEMICAL SOCIETY
Article
pubs.acs.org/JACS

High-Efficiency "Green" Quantum Dot Solar Cells

Zhenxiao Pan,[†] Iván Mora-Seró,[‡] Qing Shen,[§,¶] Hua Zhang,[†] Yan Li,[†] Ke Zhao,[†] Jin Wang,[†] Xinhua Zhong,*[,†] and Juan Bisquert[‡,∥]

[†]Key Laboratory for Advanced Materials, Institute of Applied Chemistry, East China University of Science and Technology, Shanghai 200237, China

[‡]Photovoltaic and Optoelectronic Devices Group, Department de Física, Universitat Jaume I, 12071 Castelló, Spain

[§]Department of Engineering Science, the University of Electro-Communications, 1-4-1 Chofugaoka, Chofu, Tokyo 182-8585, Japan

[¶]CREST, Japan Science and Technology Agency (JST), 4-1-8 Honcho, Kawaguchi, Saitama 332-0012, Japan

[∥]Department of Chemistry, Faculty of Science, King Abdulaziz University, Jeddah, Saudi Arabia

Supporting Information

ABSTRACT: Semiconductor quantum dots (QDs) are extremely interesting materials for the development of photovoltaic devices, but currently the present the drawback is that the most efficient devices have been prepared with toxic heavy metals of Cd or Pb. Solar cells based on "green" QDs—totally free of Cd or Pb—present a modest efficiency of 2.52%. Herein we achieve effective surface passivation of the ternary $CuInS_2$ (CIS) QDs that provides high photovoltaic quality core/shell CIS/ZnS (CIS-Z) QDs, leading to the development of high-efficiency green QD solar cells that surpass the performance of those based on the toxic cadmium and lead chalcogenides QDs. Using wide absorption range QDs, CIS-Z-based quantum dot sensitized solar cell (QDSC) configuration with high QD loading and with the benefit of the recombination reduction with type-I core/shell structure, we boost the power conversion efficiency of Cd- and Pb-free QDSC to a record of 7.04% (with certified efficiency of 6.66%) under AM 1.5G one sun irradiation. This efficiency is the best performance to date for QDSCs and also demonstrates that it is possible to obtain comparable or even better photovoltaic performance from green CIS QDs to the toxic cadmium and lead chalcogenides QDs.

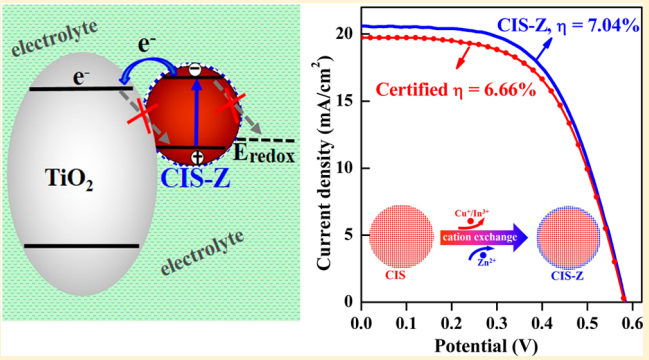

INTRODUCTION

Low-cost photovoltaic technology is an effective way to solve fossil fuel exhaustion and global warming concern.[1,2] Quantum dot (QD) solar cells are attracting increasing scientific and industrial interests as a promising low-cost candidate for the third-generation solar cell due to band gap tunability, high absorption coefficient, and solution processability.[3−8] Furthermore, multiple exciton generation phenomenon and extraction of hot electrons have the potential to be harnessed for the theoretical power conversion efficiency (PCE) of these cells to surpass the Shockley−Queisser limit (31%).[9−11] Currently, QD solar cells are mainly focused on highly toxic cadmium and lead chalcogenides,[3−8,12−14] which make the future commercial application doubtful based on health and environmental issues. In this sense, the development of a "green" alternative based on Cd- and Pb-free devices is extremely interesting.

$CuInS_2$ (CIS) QDs are an attractive less-toxic alternative to Cd- or Pb-based QDs with high absorption coefficient (~10^5 cm^{-1}) and near-optimal bulk band gap energy (1.5 eV).[15] CIS QDs have been used in the quantum dot sensitized solar cell (QDSC) configuration.[16−29] Recently great efforts, such as introducing interfacial buffer layer between QD sensitizer and TiO_2,[16−19] hybrid-sensitization with use of CdS, CdSe,[18−25] or alloying with Se, etc.,[26,27] have been devoted to enhance the photovoltaic performance of CIS-based QDSCs, but some of these strategies are not compatible with green solar cells since not totally Cd-free devices are produced. Regretfully, the appeal of CIS QD sensitizer is counterbalanced by the mean performance of the resulting cell devices with reported best PCE of 5.3%,[15] but using CdS passivation. Slightly higher efficiencies of 5.5%, 5.1% certified, have been obtained for CuInSeS QDs also with CdS passivation.[27] These efficiencies lag significantly behind those of Cd-containing QD-based QDSCs (6−7%)[30−32] or Pb-based depleted heterojunction QD solar cells (7−8%).[33,34] Furthermore, the highly toxic element cadmium is still used in almost all CIS-based QDSCs with relatively high PCE.[20−27] In the case of Cd-free, the reported best PCE is only 2.52%.[16,17,28,29] Therefore, developing Cd-, Pb-free CIS-based QDSC with good performance is critical for their commercial application and also becomes a great challenge.

Received: April 30, 2014

   dx.doi.org/10.1021/ja504310w | J. Am. Chem. Soc. XXXX, XXX, XXX−XXX

The relatively poor performance of QDSCs, especially the CIS based ones, is at least partially due to the existence of trap-state defects in QD sensitizers, which induce both internal charge carrier recombination inside QDs (before carrier injection into the transporting media) and photoexcited electron recombination from metal oxide matrix to QD sensitizer (after carrier injection), and therefore lower PCE of the resulting cell device.[35−38] Due to the high surface atom ratio and relatively low synthetic temperature, surface trapping defect is common in colloidal QDs,[39] and the situation is more severe for ternary CIS in comparison with binary II−VI QDs since ternary nanocrystals tolerate a large range of non-stoichiometric compositions and their more complex crystal structure leads to a significant density of donor and acceptor trap states located in the band gap.[40] The overgrowth of a wider band gap inorganic shell (in particular ZnS) around QDs to form type-I core/shell structure is a well-established approach to eliminate/minimize trap-state defects and improve luminescent emission efficiency and stability of QDs.[41,42] Meanwhile, surface passivation has also been extensively implemented in photoanode post-treatment by deposition of ZnS layer over the sensitized electrode via successive ionic layer adsorption and reaction (SILAR) route to reduce the QD/TiO_2/electrolyte interface recombination and therefore improve the PCE of the cell devices.[38,43−45] However, in this route ZnS can only deposit on the outer exposed surface of QD sensitizer as a loose particle-packing network and therefore cannot effectively reduce the intrinsic defect existing in QD sensitizer and cannot create a barrier at the QD/TiO_2 interface to reduce the recombination from electron in TiO_2 to hole/trap in QD.[22,37] Furthermore, to our best knowledge, the utilization of preprepared type-I core/shell QDs directly as sensitizer in QDSC has not been reported, even though the demonstration of this concept has been carried out by sensitization of TiO_2 single crystal with CdSe/ZnS QDs.[46]

Herein, we target at developing high-efficiency QDSCs based on inherently well-passivated CIS/ZnS (CIS-Z) type-I core/shell structured QD sensitizer. Oleylamine-capped CIS QDs with excitonic absorption edge extending to the near infrared (NIR) region were first prepared at high temperature. Then a thin layer of ZnS shell was overcoated around the CIS core through partial cation exchange route, followed by phase transfer via ligand exchange to get a bifunctional linker molecule mercaptopropionic (MPA)-capped water-soluble CIS-Z QDs. The hydrophilic CIS-Z QDs were immobilized onto mesoporous TiO_2 film electrode via self-assembling by dropping MPA-capped QD aqueous solution onto the film electrode. The constructed Cd-free green CIS-Z solar cell shows a best PCE of 7.04% (with certified efficiency of 6.66%) under AM 1.5 G one full sun illumination, which is a new record efficiency for green QD solar cells in any configuration and also a new record for QDSC with any QD sensitizer.[30−32]

EXPERIMENTAL SECTION

Chemicals. Indium acetate ($In(OAc)_3$, 99.99%), oleylamine (OAm, 97%), 1-octadecene (ODE, 90%), zinc acetate ($Zn(OAc)_2$, 99.99%), and sulfur powder (99.99%) were purchased from Aldrich. Copper iodide (CuI, 99.998%) and 3-mercaptopropionic acid (MPA, 97%) were obtained from Alfa Aesar. All chemicals were used as received without further processing.

Synthesis of CIS and CIS-Z QDs. For CIS QDs preparation, 14.0 mg of CuI (0.1 mmol) and 29.0 mg of $In(OAc)_3$ (0.1 mmol) were loaded in a flask containing 2.0 mL of OAm and 4.0 mL of ODE. The resulting mixture solution was subsequently heated to 180 °C under argon flow, and then 0.4 mmol of sulfur dissolved in 0.4 mL of OAm was injected into the reaction system and stayed for 20 min. The purified CIS QDs were obtained by precipitation and centrifugation procedure with use of acetone. The purified CIS QDs were dispersed in 2.0 mL of OAm and 4.0 mL of ODE and degassed under vacuum at 40 °C for 20 min. For synthesis of CIS-Z QDs with 0.7 monolayer of ZnS shell, the above solution was then heated to 100 °C and 0.04 mmol of $Zn(OAc)_2$ stock solution (obtained by dissolving 0.44 g of $Zn(OAc)_2$ in 1.6 mL of OAm and 18.4 mLof ODE) was injected into the reaction system and kept at this temperature for 30 min to employ the cation exchange procedure. After precipitation and centrifugation procedure, purified CIS-Z QDs are obtained. The ZnS thickness is dependent on both the reaction time and concentration of the Zn precursor adopted.

Sensitization of TiO_2 Film and Fabrication of Solar Cells. The preparation of TiO_2 mesoporous film electrodes (9.0 ± 0.5 μm transparent layer together with 6.0 ± 0.5 μm light scattering layer) is the same as with our previous work.[30,31] MPA-capped water-soluble QDs were obtained from the initial oil-soluble QDs via ligand exchange procedure as described previously.[47−49] QD sensitizers are immobilized on TiO_2 films by pipetting the obtained MPA-capped QD aqueous dispersion (with absorbance of 2.0 at excitonic absorption onset) onto the TiO_2 film and staying for 3 h and then rinsing with water and ethanol sequentially. After deposition, the QD-sensitized TiO_2 films were coated with ZnS for 4 cycles by dipping alternately into 0.1 M $Zn(OAc)_2$ methanol solution and 0.1 M Na_2S solutions for 1 min/dip.

The cells were constructed by assembling the brass-based Cu_2S counter electrode and QD-sensitized TiO_2 film electrode using a 50-μm thick Scotch spacer with a binder clip. The Cu_2S counter electrodes were prepared by immersing brass foil in 1.0 M HCl solution at 75 °C for 30 min. Polysulfide aqueous solution is used as electrolyte, consisting of 2.0 M Na_2S, 2.0 M S, and 0.2 M KCl. The brass foil was vulcanized immediately.

Characterization. Transition electron microscopy (TEM) images were obtained using a JEOL JEM-2100 instrument. The absorption and PL emission spectra were recorded on a Shimadzu UV-2600 and a Cary Eclipse (Varian) spectrophotometer, respectively. The $J-V$ curves of cell devices were measured using a Keithley 2400 source meter under illumination by an AM 1.5G solar simulator (Oriel, 91160). A NREL standard Si solar cell was used to calibrate the power of the simulated light to 1000 W/m^2. The photoactive area was 0.237 cm^2 defined by a black metal mask. Incident photon-to-electron conversion efficiency (IPCE) curves were measured on a Keithley 2000 multimeter under the illumination of a 300 W tungsten lamp with a Spectral Product DK240 monochromator. Electrochemical impedance spectroscopy (EIS) measurements were employed with use of an impedance analyzer (Zahner, Zennium) in dark conditions at forward bias from 0 to −0.55 V, applying a 20 mV ac sinusoidal signal over the constant applied bias with the frequency ranging from 1 MHz to 0.1 Hz. The fact that photovoltaic parameters kept nearly constant before and after EIS measurements can verify the effectiveness of the EIS data obtained. Intensity-modulated photocurrent and photovoltage spectra (IMPS/IMVS) were measured on the same electrochemical workstation (Zahner,) with a frequency response analyzer under an intensity-modulated (30−150 W

dx.doi.org/10.1021/ja504310w | J. Am. Chem. Soc. XXXX, XXX, XXX−XXX

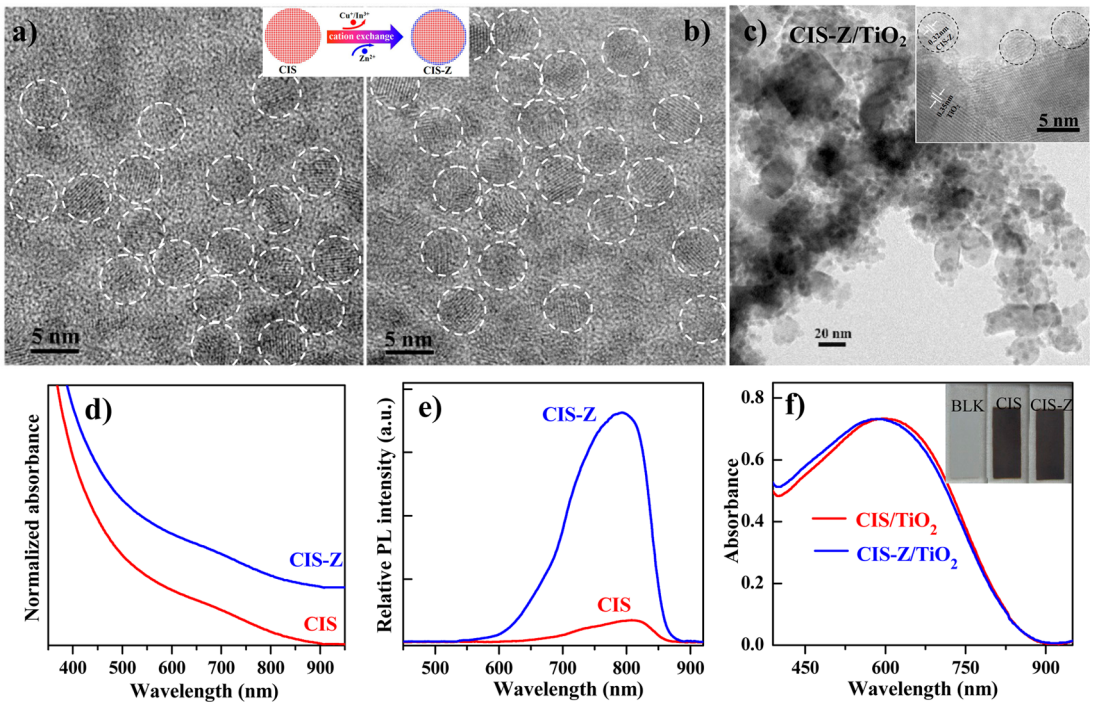

Figure 1. TEM images and optical spectra of CIS, derivative CIS-Z QD dispersions in toluene, and sensitized TiO_2 films. (a)−(b) Wide-field TEM images of CIS and CIS-Z QD dispersions, respectively. Inset illustrates the cation exchange process for CIS-Z QDs. (c) TEM images of CIS-Z QD (the small particles, ∼5 nm) sensitized TiO_2 film (the large particles ∼20 nm). Inset: HRTEM micrograph. (d)−(e) UV−vis absorption and PL emission spectra (λ_{ex} = 400 nm) of QD dispersions, respectively. (f) UV−vis absorption spectra of QD-sensitized TiO_2 film electrodes. Inset, comparative pictures of nonsensitized and sensitized electrodes with CIS and CIS-Z QDs.

m^{-2}) blue light emitting diode (457 nm) driven by a Zahner (PP211) source supply. The modulated light intensity was 10% or less than the base light intensity. The frequency range was set from 3 kHz to 0.1 Hz for IMPS and 1 kHz to 0.1 Hz for IMVS.

Two kinds of transient absorption (TA) setups were used to characterize the samples in the femtosecond (fs) and nanosecond (ns) time range. In the fs setup, the laser source was a titanium/sapphire laser (CPA-2010, Clark-MXR Inc.) with wavelength of 775 nm, repetition rate of 1 kHz, and pulse width of 150 fs. The light was separated into two parts: one as a probe pulse, the other as a pump light to pump an optical parametric amplifier (OPA) (a TOAPS from Quantronix) to generate light pulses with wavelength tunable from 290 nm to 3 μm. In this study, a pump light wavelength of 388 nm and a probe beam wavelength of 580 nm were used. In the ns TA setup, the pump light source was an OPO (Surelite II−10FP) output excited by a Nd:YAG nanosecond pulse laser (Panther, Continuum, Electro-Optics Inc.). The pulse width was 5 ns, and the repetition rate was 0.5 Hz. A pulse light with wavelength of 570 nm was used as pump light to excite the sample. The probe light was a fiber coupled CW semiconductor laser with a wavelength of 1300 nm to measure the electrons injected into TiO_2. Thus, charge recombination dynamics between the electrons in TiO_2 and holes in CIS QDs can be measured.

■ RESULTS AND DISCUSSION

In order to obtain a high-efficiency QD solar cell, QD with a broad light-harvesting range is essential. Meanwhile, in the case of QDSC configuration high QD loading is also a prerequisite for high efficiency.[38] Therefore, CIS QDs with absorption range extending to the NIR region of ∼850 nm with corresponding average size of 5.1 nm were synthesized. The synthesis of high-quality CIS QDs (high PL emission efficiency, narrow size distribution) is well-developed, but strong coordinating ligand dodecanethiol (DDT) is often used as capping reagent.[50−54] Regretfully, DDT-capped QD is difficult to immobilize on TiO_2 electrode with a high surface coverage since DDT ligand cannot be completely displaced during the phase transfer procedure due to the strong coordination capacity of the terminal thiol group.[29] This is, in part, the reason why low QD loading and poor performance were obtained when DDT-capped CIS QDs were used as sensitizer in previous reports.[25,26,28,29] This fact has pushed us to develop a DDT-free synthetic approach for CIS QDs. Briefly, NIR absorption CIS QDs were synthesized by hot injection of sulfur-oleylamine solution into octadecene (ODE) media containing CuI and $In(OAc)_3$ at 180 °C. The transmission electron microscopy (TEM) images and optical spectra of the obtained CIS QDs are shown in Figure 1. The XRD pattern as shown in Figure S1 of the Supporting Information indicates that the CIS QDs exhibit tetragonal chalcopyrite structure. It should be noted that the light absorption range of our used CIS QDs is significantly wider than those in previous reports (usually less than 700 nm). The limited light absorption range should be part of the reason for poor performance in previously reported solar cells.[16−25,28,29]

Although the CIS QDs with optimal absorption onset can be conveniently prepared via our adopted DDT-free approach, the PL quantum yield (QY) of the resulting CIS QDs is nearly zero. This indicates that high density of surface defect exists in our obtained CIS QDs.[41,42] The high defect density of QD sensitizer is fatal for the photovoltaic performance of the resulting QDSCs since the defect can serve as both internal recombination centers in QD itself, before charge injection into

dx.doi.org/10.1021/ja504310w | J. Am. Chem. Soc. XXXX, XXX, XXX−XXX

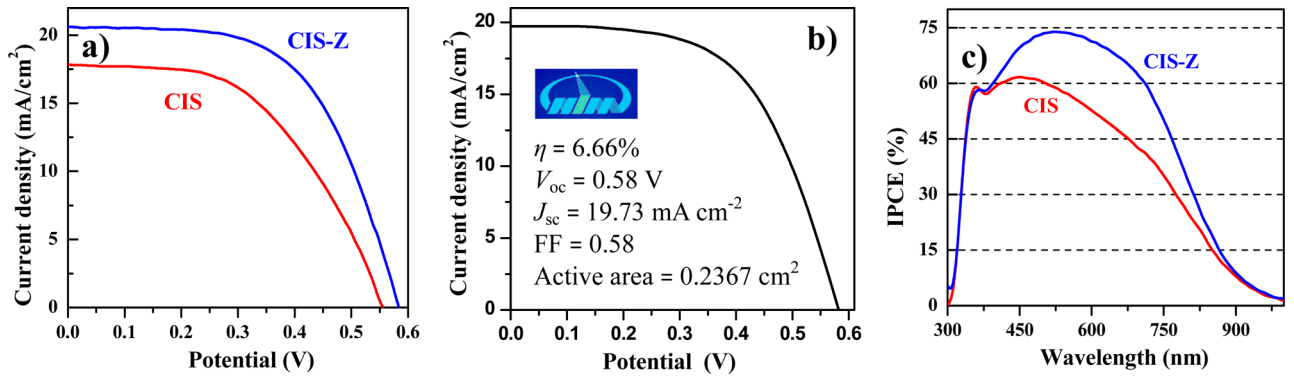

Figure 2. *J*–*V* curves of CIS-Z and CIS-based champion cells (a) and certified CIS-Z cell (b) under the irradiation of 1 full sun. (c) Incident photon to current efficiency (IPCE) curves.

the transporting media, and recombination centers from electrons already injected into the metal oxide to acceptor states in QD sensitizer or in the electrolyte. These two recombination processes reduce PCE in the resulting cell devices.[36−38]

In order to decrease the defect density, a ZnS layer was overcoated around the preprepared CIS QDs to form the CIS/ZnS core/shell QDs (noted as CIS-Z hereafter) via cation exchange by adding $Zn(OAc)_2$ into the purified CIS QDs dispersion in oleylamine at intermediate temperature, as has been discussed in the Experimental Section. This strategy for forming the core/shell heterostructure via cation exchange was extensively used in QD systems since the first report by Alivisatos.[55−57] Similar to previous reports, the adopted cation exchange route can transfer the native core QD into a similar-sized core/shell QD without enhancing the particle size due to the absence of counteranion.[55−58] This is verified by the TEM image (Figure 1a, b) of the CIS and the derived CIS-Z QDs with nearly identical average size of 5.1 ± 0.4 nm. The nonincreased size favors the immobilization of QD sensitizer onto mesoporous TiO_2 film due to the limited pore size (usually 30−50 nm) of the film. It is noted that the XRD patterns of CIS-Z QDs also show tetragonal chalcopyrite structure (Figure S1 of the Supporting Information). The Zn content in the resulting CIS-Z QDs is dependent on both the reaction time and concentration of Zn precursor adopted in the process of Zn treatment. We found that CIS-Z QDs with 20% Zn content in total cation component (based on inductively coupled plasma atomic emission spectroscopy, ICP-AES), corresponding to 0.7 monolayer of ZnS (~0.2 nm thickness), gives the best performance of the resulting cell devices as discussed below. When the Zn content is greater than 20%, the device performance decreases gradually. The PL spectra and average photovoltaic performances of CIS-Z QDs corresponding to different Zn contents are shown in Figure S2 and Table S1 of the Supporting Information, respectively. This is ascribed to the suppression of photogenerated electron injection into TiO_2 substrate due to the barrier effect of ZnS shell as discussed below. For convenience, hereafter the CIS-Z QD is specifically referred to the CIS/ZnS QD containing 20% Zn. Both absorption and PL emission spectra of CIS before and after Zn exchange show small blue-shift (<10 nm) but retain similar spectral profile (Figure 1d, e). The small blue-shift is due to shrinkage of core size and overgrowth of a thin shell of wide band gap ZnS around the core, while the PL QY of Zn-exchange CIS QD increases dramatically (more than 10-fold) after Zn exchange. The increased PL QY indicates the effective suppression of defect-trapping of the QDs.[41,42]

To evaluate the effectiveness of surface passivation of CIS QDs in the construction of high-efficiency QDSCs, we assembled both plain CIS and CIS-Z in QDSC configuration and compared their photovoltaic performance. The obtained high-quality CIS-Z and CIS QDs were tethered on TiO_2 film electrode with high surface coverage through our recently developed ex situ ligand exchange postsynthesis assembly approach, which has been proven to be an effective route for immobilizing presynthesized QD on oxide film electrode with high loading (34% coverage) and uniform distribution throughout the film thickness.[30,31,47,48] In this assembly approach, the as-prepared oil-soluble CIS-Z and CIS QDs were first made water-soluble via ligand exchange with use of bifunctional hydrophilic MPA ligand. The obtained water-soluble MPA-capped CIS and CIS-Z QD sensitizers were then immobilized onto TiO_2 film electrodes by pipetting QDs aqueous solution onto the oxide matrix and staying for 3 h. Absorption spectra of CIS and derived CIS-Z QD-sensitized TiO_2 film electrodes are shown in Figure 1f, and the corresponding photographs are shown in the inset. Similar to the case of colloidal QD dispersions (Figure 1d), the absorption spectrum of CIS-Z sensitized TiO_2 film (Figure 1f) is nearly identical to that of the CIS-based one with only a slight blue-shift. Deduced from the absorption spectra, the light-harvesting range of both sensitized films covers the whole visible spectrum and extends to the NIR region with wavelength as far as 900 nm. This wide absorption feature is further verified by the black color of the sensitized films as shown in the inset of Figure 1f. This broad absorption spectral range paves the way for high photocurrent in the resulting cell devices as discussed below. The relatively high absorbance by these sensitized film electrodes indicates high QDs loading, which could be visualized by the deep coloration as shown in the inset of Figure 1f.

TEM images (Figure 1c) of CIS-Z QD-sensitized TiO_2 film show the size of QD sensitizers and their distribution on the TiO_2 matrix. From the wide-field TEM images, it can be found that the surface of TiO_2 particles (larger particles ~20−40 nm) is covered densely by smaller dots (CIS-Z QD, ~5 nm), demonstrating a high coverage of the surface of TiO_2 film, in good agreement with the absorption spectra. Meanwhile, the size of most CIS-Z QDs deposited was nearly monodisperse, and the shape was nearly spherical. Furthermore, single monolayer of QD sensitizer on the oxide surface similar to the case of molecule dyes is also achieved. The HRTEM image

dx.doi.org/10.1021/ja504310w | J. Am. Chem. Soc. XXXX, XXX, XXX−XXX

in the inset of Figure 1c shows clearly the crystalline lattice fringes of the TiO_2/CIS-Z composite. The anatase TiO_2 substrate displays the (101) plane with lattice spacing distance of 0.35 nm, while the tetragonal crystal phase CIS-Z QDs display the (112) plane of 0.32 nm spacing distance.

Photovoltaic Performance. After deposition of MPA-capped water-soluble QDs, a thin passivation layer of ZnS was further deposited onto the QD-sensitized TiO_2 films via the successive ionic layer absorption and reaction (SILAR) route according to standard literature method.[38,43−45] Then sandwich-type cells were constructed using Cu_2S on brass foil as counter electrode and polysulfide electrolyte (2.0 M Na_2S, and 2.0 M S in aqueous solution) as hole transporting media. The current density−voltage (J−V) curves of both CIS and CIS-Z champion cells under the irradiation of 1 full sun intensity (measured with mask, AM 1.5G at 100 mW cm^{-2}) are shown in Figure 2a, and the average values for main photovoltaic parameters based on six cell devices in parallel are listed in Table 1. The J−V curves and photovoltaic parameters for each tested cells are available in Figure S3 and Table S2 of the Supporting Information, respectively. It is highlighted that the small standard deviation obtained here indicates the high reproducibility of the method used for construction of cell devices. A representative CIS-Z cell was sent to the National Institute of Metrology (NIM), China for certification, and the certified PCE was 6.66% (Figure 2b, Table 1, the detailed information is available in the Supporting Information). In comparison, all the averaged photovoltaic parameters (short-circuit current J_{sc}, open-circuit voltage V_{oc}, and fill factor FF) for CIS-Z cell are enhanced 10−15% in comparison with those of CIS. The observed enhanced photovoltaic performances of CIS-Z cells are mainly attributed to the surface passivation and accordingly the reduction of charge carrier recombination as discussed below. To our best knowledge, both our measured PCE of 7.04% and the certified PCE of 6.66% are the highest reported values not only for green QD solar cells but also in all QDSCs so far. It is noted that other types of quantum dot solar cells, but using depleted heterojunction configuration based on PbS and solid-state based on Sb_2S_3, have attained PCE values of 6−8%.[31,32,59] Our results reported here push the efficiencies reported for green QDs in the same range as other QDs photovoltaic technology containing toxic Cd or Pb.

Table 1. Photovoltaic Parameters Extracted from J−V Measurements

QDs	J_{sc} (mA·cm^{-2})	V_{oc} (V)	FF	η (%)
CIS-Z[a]	20.65	0.586	0.581	7.04
CIS-Z[b]	19.73	0.580	0.580	6.66
CIS-Z[c]	20.26	0.584	0.575	6.83 ± 0.12
CIS[a]	17.82	0.555	0.511	5.05
CIS[c]	17.92	0.541	0.491	4.82 ± 0.12

[a]Performance of champion cells. [b]Certified cell. [c]Average value of six devices in parallel.

Incident photon-to-electron conversion efficiency (IPCE, also referred as external quantum efficiency, EQE) is plotted in Figure 2c. It was found that the overall photocurrent response closely matches the corresponding absorption spectra of QD-sensitized TiO_2 films as shown in Figure 1f, and the photocurrent response starts at near 950 nm for both CIS and CIS-Z based cells. By integrating the product of the incident photon flux density and the cell's IPCE spectra, the calculated J_{sc} for CIS-Z and CIS cells is 19.5 and 17.3 mA·cm^{-2}, respectively, in good agreement with the measured values; see Table 1. The IPCE values for CIS-Z are remarkablely higher than those of CIS in the whole photoresponse range. More than 60% of IPCE value in a wide range between 350 and 700 nm has been achieved for CIS-Z sensitizers with highest value approaching 75%. The low IPCE values in the range of 700−900 nm for both cells could be ascribed to the smaller absorbance or light-harvesting efficiency (LHE) in this spectral region as shown in Figure 1f.

It has been established that IPCE can be calculated from the equation IPCE = LHE × ϕ_{inj} × η_c,[60] where ϕ_{inj} is the electron injection efficiency and η_c is charge collection efficiency. As shown in Figure 1f, CIS- and CIS-Z sensitized TiO_2 films show a similar spectral profile, indicating that both sensitized films show similar light-harvesting capability, i.e, similar LHE value. In order to evaluate the effect of the other two contributions (i.e., ϕ_{inj} and η_c) to the IPCE, electrochemical impedance spectroscopy (EIS) and transient absorption (TA) characterization have been carried out.

Electrochemical Impedance Spectroscopy. EIS was employed to unveil the intrinsic mechanism of the better photovoltaic performance of the CIS-Z solar cells related to reference CIS cells with use of the standard models developed by ourselves.[38,61−63] The detailed Nyquist curves under different bias for both CIS-Z and CIS cells are available in Figure S4 of the Supporting Information. The chemical capacitance C_μ, and recombination resistance R_{rec} extracted

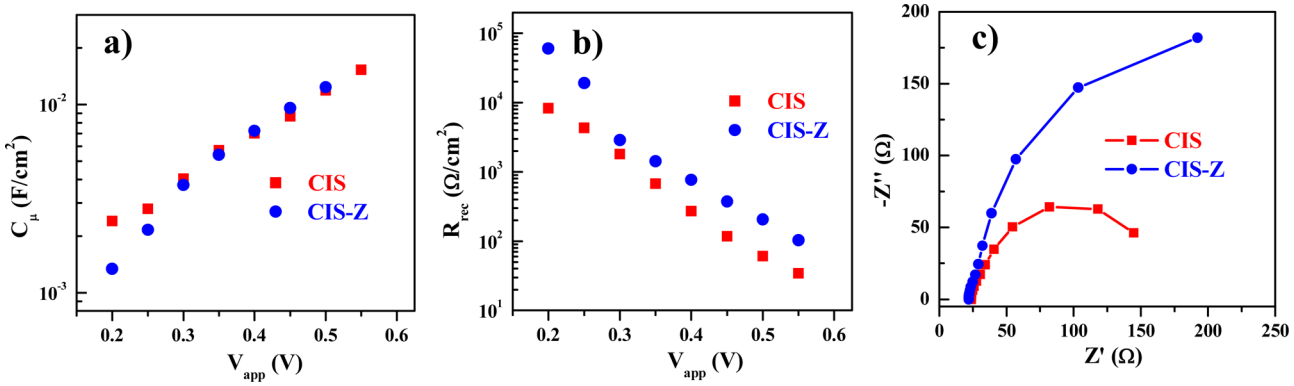

Figure 3. Electrochemical impedance spectroscopy characterization of the CIS-Z and reference CIS QD based cells. (a) Dependence of chemical capacitance C_μ and (b) recombination resistance R_{rec} on applied voltage (V_{appl}). (c) Nyquist plots of both cells at −0.55 V forward bias.

dx.doi.org/10.1021/ja504310w | J. Am. Chem. Soc. XXXX, XXX, XXX−XXX

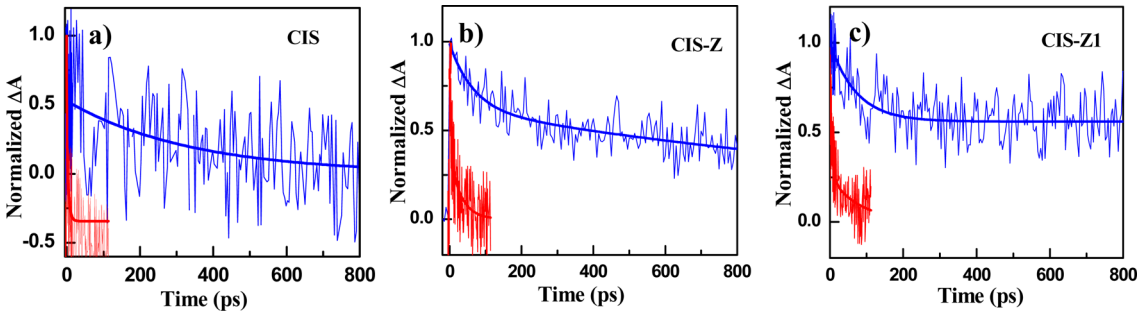

Figure 4. Transient absorption characterization in picosecond time scale. Kinetic traces of the excitonic decay (recorded at 580 nm) of (a) CIS, (b) CIS-Z, and (c) CIS-Z1 QDs deposited on SiO_2 (blue fine lines) and TiO_2 substrates (red fine lines) for a time scale up to 800 ps. The bold lines represent the corresponding biexponential fit, eq 1. All measurements were carried out in N_2 atmosphere using a 388 nm laser pulse excitation.

Table 2. Fitting Results of the TA Responses with Biexponential Function Eq 1 and Calculated Average Lifetime Using Eq 2 as Well as Electron Injection Rate Calculated Using Eq 3

samples	t_1 (ps)	t_2 (ps)	A_1	A_2	t_{av} (ps)	k_{ET} ($\times 10^{11}$ s^{-1})
SiO_2/CIS	2.4 ± 1.8	359 ± 125	0.60 ± 0.28	0.40 ± 0.08	355.5	
SiO_2/CIS-Z	66 ± 19	1769 ± 307	0.37 ± 0.05	0.63 ± 0.03	1732.5	
SiO_2/CIS-Z1	72 ± 17	≫1 ns	0.44 ± 0.04	0.56 ± 0.03	≫1 ns	
TiO_2/CIS	0.15 ± 0.11	4.9 ± 0.9	0.54 ± 0.2	0.46 ± 0.07	4.7	2.08
TiO_2/CIS-Z	4.3 ± 1.3	32 ± 8	0.57 ± 0.08	0.43 ± 0.08	27.8	0.35
TiO_2/CIS-Z1	5.7 ± 1.3	83 ± 32	0.69 ± 0.06	0.31 ± 0.06	72.8	0.14

from the corresponding Nyquist curves are illustrated in Figure 3a, b. It has been well established that R_{rec} in QDSCs reflects the charge recombination process between QD sensitizers/TiO_2/electrolyte interfaces.[38,61] The similar C_μ values observed in both cells (Figure 3a) indicate that the nature of the different sensitizers (CIS or CIS-Z QDs) does not affect the position of the conduction band edge or the density of states of TiO_2.[38] As shown in Figure 3b, the difference in R_{rec} values between the two cells in the whole applied forward bias range is remarkable. The R_{rec} values of CIS-Z cells are several times higher than those of CIS cells. For clarity, Figure 3c gives direct comparison of Nyquist plots between CIS-Z and CIS cells at forward bias of −0.55 V, which is near the V_{oc} values of the two cells, and the extracted EIS parameters are collected in Table S3 of the Supporting Information. We can find that the R_{rec} value of CIS-Z cell is nearly threefold to that of CIS cells. Because of the identical device structure (i.e., identical TiO_2 film electrode and redox electrolyte), there is no difference in the recombination of photoexcited electrons at the metal oxide matrix with acceptor species in electrolyte between two cells. Therefore, the observed greater recombination resistance in CIS-Z cell related to CIS cell should be ascribed to the blockage of electron recombination between TiO_2/QD interface and/or QD/electrolyte interface, i.e., the back electron transfer from TiO_2 to QD sensitizer and/or from QD to electrolyte. This is further verified by the TA measurements below. As described above, the passivation of ZnS around the CIS core suppresses the surface traps and then switches off the back electron transfer routes. Meanwhile, the calculated electron lifetime ($\tau_n = R_{rec} \times C_\mu$) for the CIS-Z cell at open-circuit condition is ∼threefold longer than that of the CIS cell, which favors the improvement of charge collection efficiency, η_c. These results are also supported by intensity modulated photocurrent/photovoltage spectroscopy (IMPS/IMVS) and transient absorption in the microsecond−millisecond range; see the Supporting Information.

TA Measurement. To study the photoexcited carrier dynamics in CIS-Z QDs and electron injection rate from CIS-Z QDs to TiO_2 substrates as well as the effects of ZnS passivation on them, we used femtosecond (fs) and nanosecond (ns) transient absorption (TA) setups to characterize the charge separation (i.e., electron injection) and recombination dynamics for CIS QDs and CIS QDs with different thickness of ZnS coatings deposited on insulating SiO_2 films or TiO_2 films (SiO_2/CIS, TiO_2/CIS, SiO_2/CIS-Z, TiO_2/CIS-Z, SiO_2/CIS-Z1, TiO_2/CIS-Z1, CIS-Z, and CIS-Z1 correspond to ZnS shell thickness of 0.7 and 1.5 ML, respectively).[64,65] The pump light wavelength is 388 nm and the probe light wavelength is 580 nm, which are identical to the TA spectra of CIS QDs reported by Kamat.[25] Similarly, we observed a bleaching of the ground-state absorption as the charge-separation state created after pump light was absorbed. With increasing time, the bleached absorption recovers as the electrons recombine with the holes. Figure 4 shows the normalized TA decay signals of the six studied samples, which correspond to kinetic traces of the excitonic decay for different QDs deposited on the two different substrates. It can be found that for all studied QDs on insulating SiO_2, the recovery of the bleaching is rather slow since the charge recombination in all QDs is dominated by electron in the conduction band and hole in the valence band, including those through surface defect states and direct recombination between electrons and holes and there is no electron injection from CIS QDs to the insulating SiO_2. However, the recovery of QDs bleaching on TiO_2 is much faster, which indicates that a fast electron-transfer is dominated. We find that there are two decay processes in all the TA kinetics, and they can be fitted very well to a biexponential function of eq 1

$$Y = A_1 e^{-t/t_1} + A_2 e^{-t/t_2} \quad (1)$$

where t_1 and t_2 are the lifetimes and A_1 and A_2 are the contributions from the two components. Table 2 shows the fitting results of all the samples. For CIS/SiO_2 sample, the two

dx.doi.org/10.1021/ja504310w | J. Am. Chem. Soc. XXXX, XXX, XXX−XXX

lifetimes are 2.4 and 359 ps, respectively. As discussed earlier, there are a lot of defects for CIS QDs without ZnS passivation. Thus, the fast and slow decay processes can be considered to result from recombination through shallow and deep defects. As ZnS passivation with a thinner thickness (SiO_2/CIS-Z sample), the two lifetimes increased greatly up to 66 ps and 1.7 ns, respectively. As ZnS thickness was increased more (SiO_2/CIS-Z1), the fast lifetime was almost the same as that of SiO_2/CIS-Z1; however, the lifetime for the slow one became much longer than 1 ns. These results demonstrate that the surface defects decreased dramatically by the ZnS passivation on the CIS QD surfaces, which is consistent with the PL results mentioned above. For TiO_2 substrate, t_1 and t_2 for samples CIS, CIS-Z, and CIS-Z1 follow the same trend but with a dramatic decrease of the lifetime; see Table 2. Then, we calculated the average lifetimes of the photoexcited carriers using eq 2[66]

$$t_{av} = \frac{A_1 t_1^{\,2} + A_2 t_2^{\,2}}{A_1 t_1 + A_2 t_2} \quad (2)$$

The results of t_{av} for each sample are shown in Table 2. Very interestingly, as the ZnS coating was applied to the QD surface, t_{av} increases 1 order of magnitude, showing a dramatic decrease in the internal recombination (before charge injection into TiO_2) and consequently increase of the electron injection efficiency ϕ_{inj}. The electron injection rate constant k_{ET} can be obtained from eq 3 as follows:[66]

$$vk_{ET} = 1/t_{av(CIS/TiO_2)} - 1/t_{av(CIS/SiO_2)} \quad (3)$$

The result of k_{ET}, shown in Table 2, is 2×10^{11} s^{-1} for CIS QDs without ZnS surface coating, which is in good agreement with the reported results.[25,34] With ZnS coating k_{ET} decreases as ZnS shell acts also as a barrier for carrier injection. In this sense, ZnS shell has two conflicting effects that must be conveniently balanced in order to increase ϕ_{inj}. On one hand ZnS reduces internal recombination and on the other one it acts as injection barrier. Optimum behavior has been obtained for 0.7 ML ZnS shell.

CONCLUSIONS

We have developed high-efficiency green QDSC based on CIS-Z QD sensitizer. These solar cells show an unprecedented champion cell efficiency of 7.04% and a certified efficiency of 6.66%, a record efficiency for Cd- and Pb-free QD solar cells, and the highest efficiency ever reported for QDSCs. The huge increase in the efficiency for green QDs solar cells is based on (i) the use of CIS QDs with broad light absorption range extending to NIR; (ii) preparation of type-I CIS/ZnS core/shell QDs; this ZnS shell coating increases significantly the electron injection efficiency ϕ_{inj}, and charge collection efficiency, η_c, as demonstrated by TA and EIS characterization respectively; and (iii) a high QD loading by linker molecule exchange, that allows a high light-harvesting efficiency, LHE. These results place Cd- and Pb-free QD solar cells for the first time at the same level of efficiency as their counterparts containing these toxic elements, opening a broad range of possibilities for further enhancement of friendly materials for QD photovoltaics. We are confident that with the optimization of redox electrolyte and corresponding counter electrode,[67] the photovoltaic performances of QDSCs can catch or even surpass those of its analogue dye-sensitized solar cells.

ASSOCIATED CONTENT

Supporting Information

XRD patterns of CIS and CIS-Z QDs; $J-V$ curves and photovoltaic parameters of CIS and CIS-Z with different Zn contents based cell devices (each group has six devices in parallel); certified report for photovoltaic performance of CIS-Z cell; Nyquist curves under different bias voltages for both CIS and CIS-Z cells and the EIS parameters at forward bias of −0.55 V; intensity-modulated photocurrent/photovoltage spectroscopy (IMPS/IMVS); ns-TA measurements. This material is available free of charge via the Internet at http://pubs.acs.org.

AUTHOR INFORMATION

Corresponding Author

zhongxh@ecust.edu.cn.

Notes

The authors declare no competing financial interest.

ACKNOWLEDGMENTS

We acknowledge the National Natural Science Foundation of China (Nos. 21175043, 21301059), the Science and Technology Commission of Shanghai Municipality (11JC1403100, 12NM0504101, 12ZR1407700), and the Fundamental Research Funds for the Central Universities for financial support.

REFERENCES

(1) Swierk, J. R.; Mallouk, T. E. *Chem. Soc. Rev.* **2013**, *42*, 2357−2387.
(2) Bai, Y.; Mora-Seró, I.; Angelis, F. D.; Bisquert, J.; Wang, P. *Chem. Rev.* **2014**, DOI: 10.1021/cr400606n.
(3) Kamat, P. V. *J. Phys. Chem. Lett.* **2013**, *4*, 908−918.
(4) Kramer, I. J.; Sargent, E. H. *Chem. Rev.* **2014**, *114*, 863−882.
(5) Albero, J.; Clifford, J. N.; Palomares, E. *Coord. Chem. Rev.* **2013**, *263−264*, 53−64.
(6) Lohse, S. E.; Murphy, C. J. *J. Am. Chem. Soc.* **2012**, *134*, 15607−15620.
(7) Kamat, P. V.; Tvrdy, K.; Baker, D. R.; Radich, J. G. *Chem. Rev.* **2010**, *110*, 6664−6688.
(8) Ruhle, S.; Shalom, M.; Zaban, A. *ChemPhysChem* **2010**, *11*, 2290−2304.
(9) Nozik, A. J.; Beard, M. C.; Luther, J. M.; Law, M.; Ellingson, R. J.; Johnson, J. C. *Chem. Rev.* **2010**, *110*, 6873−6890.
(10) Sambur, J. B.; Novet, T.; Parkinson, B. A. *Science* **2010**, *330*, 63−66.
(11) Semonin, O. E.; Luther, J. M.; Choi, S.; Chen, H.-Y.; Gao, J.; Nozik, A. J.; Beard, M. C. *Science* **2011**, *334*, 1530−1533.
(12) Yang, Z.; Chen, C.-Y.; Roy, P.; Chang, H.-T. *Chem. Commun.* **2011**, *47*, 9561−9571.
(13) Kamat, P. V. *J. Phys. Chem. C* **2008**, *112*, 18737−18753.
(14) Mora-Seró, I.; Bisquert, J. *J. Phys. Chem. Lett.* **2010**, *1*, 3046−3052.
(15) Booth, M.; Brown, A. P.; Evans, S. D.; Critchley, K. *Chem. Mater.* **2012**, *24*, 2064−2070.
(16) Chang, J.-Y.; Su, L.-F.; Li, C.-H.; Chang, C.-C.; Lin, J.-M. *Chem. Commun.* **2012**, *48*, 4848−4850.
(17) Wang, Y.; Rui, Y.; Zhang, Q.; Li, Y.; Wang, H. *ACS Appl. Mater. Interfaces* **2013**, *5*, 11858−11864.
(18) Xu, G.; Ji, S.; Miao, C.; Liu, G.; Ye, C. *J. Mater. Chem.* **2012**, *22*, 4890−4896.
(19) Chang, J. Y.; Lin, J. M.; Su, L. F.; Chang, C. F. *ACS Appl. Mater. Interfaces* **2013**, *5*, 8740−8752.
(20) Luo, J.; Wei, H.; Huang, Q.; Hu, X.; Zhao, H.; Yu, R.; Li, D.; Luo, Y.; Meng, Q. *Chem. Commun.* **2013**, *49*, 3881−3883.
(21) Hu, X.; Zhang, Q.; Huang, X.; Li, D.; Luo, Y.; Meng, Q. *J. Mater. Chem.* **2011**, *21*, 15903−15905.

(22) Li, T. L.; Lee, Y. L.; Teng, H. S. *Energy Environ. Sci.* **2012**, *5*, 5315−5324.
(23) Lin, C. Y.; Teng, C. Y.; Li, T. L.; Lee, Y. L.; Teng, H. S. *J. Mater. Chem. A* **2013**, *1*, 1155−1162.
(24) Li, T. L.; Lee, Y. L.; Teng, H. S. *J. Mater. Chem.* **2011**, *21*, 5089−5098.
(25) Santra, P. K.; Nair, P. V.; Thomas, K. G.; Kamat, P. V. *J. Phys. Chem. Lett.* **2013**, *4*, 722−729.
(26) McDaniel, H.; Fuke, N.; Pietryga, J. M.; Klimov, V. I. *J. Phys. Chem. Lett.* **2013**, *4*, 355−361.
(27) McDaniel, H.; Fuke, N.; Makarov, N. S.; Pietryga, J. M.; Klimov, V. I. *Nat. Commun.* **2013**, *4*, 2887.
(28) Peng, Z.; Liu, Y.; Zhao, Y.; Shu, W.; Chen, K.; Bao, Q.; Chen, W. *Electrochim. Acta* **2013**, *111*, 755−761.
(29) Chang, C. C.; Chen, J. K.; Chen, C. P.; Yang, C. H.; Chang, J. Y. *ACS Appl. Mater. Interfaces* **2013**, *5*, 11296−11306.
(30) Wang, J.; Mora-Sero, I.; Pan, Z.; Zhao, K.; Zhang, H.; Feng, Y.; Yang, G.; Zhong, X.; Bisquert, J. *J. Am. Chem. Soc.* **2013**, *135*, 15913−15922.
(31) Pan, Z.; Zhao, K.; Wang, J.; Zhang, H.; Feng, Y.; Zhong, X. *ACS Nano* **2013**, *7*, 5215−5222.
(32) Yan, K.; Zhang, L.; Qiu, J.; Qiu, Y.; Zhu, Z.; Wang, J.; Yang, S. *J. Am. Chem. Soc.* **2013**, *135*, 9531−9539.
(33) Ning, Z.; Zhitomirsky, D.; Adinolfi, V.; Sutherland, B.; Xu, J.; Voznyy, O.; Maraghechi, P.; Lan, X.; Hoogland, S.; Ren, Y.; Sargent, E. H. *Adv. Mater.* **2013**, *25*, 1719−1723.
(34) Ip, A. H.; Thon, S. M.; Hoogland, S.; Voznyy, O.; Zhitomirsky, D.; Debnath, R.; Levina, L.; Rollny, L. R.; Carey, G. H.; Fischer, A.; Kemp, K. W.; Kramer, I. J.; Ning, Z.; Labelle, A. J.; Chou, K. W.; Amassian, A.; Sargent, E. H. *Nat. Nanotechnol.* **2012**, *7*, 577−582.
(35) Roelofs, K. E.; Brennan, T. P.; Bent, S. F. *J. Phys. Chem. Lett.* **2014**, *5*, 348−360.
(36) Kamat, P. V. *Acc. Chem. Res.* **2012**, *45*, 1906−1915.
(37) Hodes, G. *J. Phys. Chem. C* **2008**, *112*, 17778−17787.
(38) Mora-Seró, I.; Gimenez, S.; Fabregat-Santiago, F.; Gomez, R.; Shen, Q.; Toyoda, T.; Bisquert, J. *Acc. Chem. Res.* **2009**, *42*, 1848−1857.
(39) Alivisatos, A. P. *Science* **1996**, *271*, 933−937.
(40) Aldakov, D.; Lefrançois, A.; Reiss, P. *J. Mater. Chem. C* **2013**, *1*, 3756−3776.
(41) Chaudhuri, R. G.; Paria, S. *Chem. Rev.* **2012**, *112*, 2373−2433.
(42) Dabbousi, B. O.; Rodriguez-Viejo, J.; Mikulec, F. V.; Heine, J. R.; Mattoussi, H.; Ober, R.; Jensen, K. F.; Bawendi, M. G. *J. Phys. Chem. B* **1997**, *101*, 9463−9475.
(43) Diguna, L. J.; Shen, Q.; Kobayashi, J.; Toyoda, T. *Appl. Phys. Lett.* **2007**, *91*, 023116.
(44) Barea, E. M.; Shalom, M.; Gimenez, S.; Hod, I.; Mora-Seró, I.; Zaban, A.; Bisquert, J. *J. Am. Chem. Soc.* **2010**, *132*, 6834−6839.
(45) Guijarro, N.; Campina, J. M.; Shen, Q.; Toyoda, T.; Lana-Villarreala, T.; Gomez, R. *Phys. Chem. Chem. Phys.* **2011**, *13*, 12024−12032.
(46) Sambur, J. B.; Parkinson, B. A. *J. Am. Chem. Soc.* **2010**, *132*, 2130−2131.
(47) Zhang, H.; Cheng, K.; Hou, Y.; Fang, Z.; Pan, Z.; Wu, W.; Hua, J.; Zhong, X. *Chem. Commun.* **2012**, *48*, 11235−11237.
(48) Pan, Z.; Zhang, H.; Cheng, K.; Hou, Y.; Hua, J.; Zhong, X. *ACS Nano* **2012**, *6*, 3982−3991.
(49) Liu, L.; Guo, X.; Li, Y.; Zhong, X. *Inorg. Chem.* **2010**, *49*, 3768−3775.
(50) Li, L.; Pandey, A.; Werder, D. J.; Khanal, B. P.; Pietryga, J. M.; Klimov, V. I. *J. Am. Chem. Soc.* **2011**, *133*, 1176−1179.
(51) Xie, R.; Rutherford, M.; Peng, X. *J. Am. Chem. Soc.* **2009**, *131*, 5691−5697.
(52) Zhong, H.; Lo, S. S.; Mirkovic, T.; Li, Y.; Ding, Y.; Li, Y.; Scholes, G. D. *ACS Nano* **2010**, *4*, 5253−5262.
(53) Chen, B.; Zhong, H.; Zhang, W.; Tan, Z.; Li, Y.; Yu, C.; Zhai, T.; Bando, Y.; Yang, S.; Zou, B. *Adv. Funct. Mater.* **2012**, *22*, 2081−2088.
(54) Zhang, W.; Zhong, X. *Inorg. Chem.* **2011**, *50*, 4065−4072.
(55) Park, J.; Kim, S. W. *J. Mater. Chem.* **2011**, *21*, 3745−3750.
(56) Tang, J.; Kemp, K. W.; Hoogland, S.; Jeong, K. S.; Liu, H.; Levina, L.; Furukawa, M.; Wang, X.; Debnath, R.; Cha, D.; Chou, K.; Fischer, A.; Amassian, A.; Asbury, J. B.; Sargent, E. H. *Nat. Mater.* **2011**, *10*, 765−771.
(57) Son, D. H.; Hughes, S. M.; Yin, Y.; Alivisatos, A. P. *Science* **2004**, *306*, 1009−1012.
(58) Zhong, X.; Feng, Y.; Zhang, Y.; Gu, Z.; Zou, L. *Nanotechnology* **2007**, *18*, 385606.
(59) Im, S. H.; Lim, C.-S.; Chang, J. A.; Lee, Y. H.; Maiti, N.; Kim, H.-J.; Nazeeruddin, Md. K.; Gratzel, M.; Seok, S. I. *Nano Lett.* **2011**, *11*, 4789−4793.
(60) Fillinger, A.; Parkinson, B. A. *J. Electrochem. Soc.* **1999**, *146*, 4559−4564.
(61) González-Pedro, V.; Xu, X.; Mora-Seró, I.; Bisquert, J. *ACS Nano* **2010**, *4*, 5783−5790.
(62) Kim, H.-S.; Mora-Seró, I.; Gonzalez-Pedro, V.; Fabregat-Santiago, F.; Juarez-Perez, E. J.; Park, N.-G.; Bisquert, J. *Nat. Commun.* **2013**, *4*, 2242.
(63) Fabregat-Santiago, F.; Garcia-Belmonte, G.; Mora-Seró, I.; Bisquert, J. *Phys. Chem. Chem. Phys.* **2011**, *13*, 9083−9118.
(64) Shen, Q.; Ogomi, Y.; Park, B. W.; Inoue, T.; Pandey, S. S.; Miyamoto, A.; Fujita, S.; Katayama, K.; Toyoda, T.; Hayase, S. *Phys. Chem. Chem. Phys.* **2012**, *14*, 4605−4613.
(65) Shen, Q.; Ogomi, Y.; Das, S. K.; Pandey, S. S.; Yoshino, K.; Katayama, K.; Momose, H.; Toyoda, T.; Hayase, S. *Phys. Chem. Chem. Phys.* **2013**, *15*, 14370−14376.
(66) Guijarro, N.; Lana-Villarreal, T.; Shen, Q.; Toyoda, T.; Gómez, R. *J. Phys. Chem. C* **2010**, *114*, 21928−21937.
(67) Zhao, K.; Yu, H.; Zhang, H.; Zhong, X. *J. Phys. Chem. C* **2014**, *118*, 5683−5690.